Crystal Structures of Two Self-Hydroxylating Ribonucleotide Reductase Protein R2 Mutants: Structural Basis for the Oxygen-Insertion Step of Hydroxylation Reactions Catalyzed by Diiron Proteins[†,||]

Derek T. Logan,[‡] Fredrick deMaré,[§] Bert O. Persson, Agneta Slaby, Britt-Marie Sjöberg, and Pär Nordlund*[,‡]

Department of Molecular Biology, University of Stockholm, S-106 91 Stockholm, Sweden

Received March 19, 1998; Revised Manuscript Received May 21, 1998

ABSTRACT: The R2 protein of ribonucleotide reductase catalyzes the dioxygen-dependent one-electron oxidation of Tyr122 at a diiron-carboxylate site. Methane monooxygenase and related hydroxylases catalyze hydrocarbon hydroxylation at diiron sites structurally related to the one in R2. In protein R2, the likely reaction site for dioxygen is close to Phe208. The crystal structure of an iron ligand mutant R2, Y122F/E238A, reveals the hydroxylation of Phe208 at the meta, or ϵ-, ring position and the subsequent coordination of this residue to the diiron site. In another mutant, F208Y, the "foreign" residue Tyr208 is hydroxylated to Dopa. The structures of apo and diferrous F208Y presented here suggest that Tyr208 is coordinated to the iron site of F208Y throughout the Dopa generation cycle. Together, the structural data on these two mutants suggest two possible reaction geometries for the hydroxylation reaction catalyzed by these modified R2 diiron sites, geometries which might be relevant for the hydroxylation reaction catalyzed by other diiron sites such as methane monooxygenase. A critical role for residue Glu238 in directing the oxidative power of the reactive intermediate toward oxidation of Tyr122 is proposed.

Diiron-carboxylate proteins constitute a diverse family of proteins, of which most members catalyze dioxygen-dependent hydroxylation or oxidation chemistry (*1*). The prototype members of this family are: ribonucleotide reductase protein R2 (RNR[1] R2) (*2*−*4*), generating a catalytically essential tyrosyl radical; methane monooxygenase (MMO), a promiscuous hydroxylase/oxidase (*5*, *6*); Δ9 stearoyl-acyl carrier protein desaturase, a fatty acid oxidase in plants (*7*); bacterioferritin, a ferroxidase (*8*); rubrerythrin, a possible ferroxidase in anaerobic bacteria (*9*); hemerythrin, an oxygen carrier in marine invertebrates (*10*); and purple acid phosphatase, which catalyzes phosphoryl transfer reactions (*11*). The first three of these enzyme families have been shown to be structurally and possibly evolutionarily related (*1*), and all catalyze oxygen-dependent reactions.

Ribonucleotide reductases catalyze the formation of deoxyribonucleotide DNA precursors using a radical mechanism. In the class I RNRs found in some prokaryotes (including *Escherichia coli*) and in eukaryotes, the enzyme is formed by two homodimeric proteins R1 and R2 (*4*). R1 carries the substrate and allosteric effector binding sites, while RNR R2 is the site for the generation and stabilization of the catalytic tyrosyl radical located on Tyr122. Subunit R2 is highly α-helical, having a diiron site buried in a 4α helix bundle. The iron coordination is dominated by carboxylate ligands, and Tyr122 is located near the diiron site (*2*).

In the radical generation reaction, the ferrous form of the diiron-carboxylate cluster first reacts with dioxygen. In subsequent steps, several different iron-oxo intermediates, including high-valent iron species, are formed, leading to fully reduced oxygen, a diferric iron-oxo site, and an oxidized tyrosyl radical at Tyr122. The initial source of the oxo bridge is molecular oxygen (*12*). When Tyr122 is mutated to Phe, the oxidative power of the diiron-oxo intermediates is often redirected to form other transient radical species on, e.g., tryptophan residues in the neighborhood of the diiron site (*13*, *14*).

One face of the diiron site points into a hydrophobic pocket formed by Ile234, Phe212, and Phe208. This is the most likely site for the oxygen reaction to take place, since there are accessible positions for initial dioxygen coordination as well as subsequent coordination of reactive oxygen species (*15*). In a mutant R2 where Phe208 was substituted with tyrosine, Tyr208 was transformed into Dopa (dihydroxyphenylalanine) (*16*, *17*). The structure of Dopa-containing F208Y revealed the Dopa to be coordinated in a semibridging chelating mode at the diiron site (*15*). The oxygen atom

[†] This work was supported by grants from the Swedish National Board for Technical and Industrial Development (NUTEK) and the Swedish Research Council for Engineering Sciences (TFR) to B.-M.S. and from the Swedish Research Council for Natural Sciences (NFR) to P.N.

[||] Data for mutant Y122F/E238A have been submitted to the Protein Data Bank. Accession numbers are 1BIQ for the coordinates and R1BIQSF for the structure factors.

* To whom correspondence should be addressed. Telephone: (+46) 8 16 41 41. Fax: (+46) 8 15 36 79. E-mail: par@biokemi.su.se.-

[‡] Current address: Department of Biochemistry, Stockholm University, S-106 91 Stockholm, Sweden.

[§] Current address: Biotechnology/Expression, Pharmacia and Upjohn AB, S-112 87 Stockholm, Sweden.

[1] Abbreviations: RNR, ribonucleotide reductase; MMO, methane monooxygenase; Dopa, dihydroxyphenylalanine; MMOH, methane monooxygenase hydroxylase; PAP, purple acid phosphatase; LMCT, ligand-to-metal charge transfer; OHW, "oxo−hydroxo−water"; EDTA, ethylenediaminetetraacetatic acid; CCP4, Collaborative Computer Project no. 4; MES, 2-(*N*-morpholino)ethanesulfonic acid.

S0006-2960(98)00640-0 CCC: $15.00
Published on Web 07/10/1998

inserted into Tyr208 was, somewhat surprisingly, shown to originate from a water molecule and not from dioxygen (*16*). Quinone cofactors similar to Dopa122 have been found in many proteins. It has been shown that these cofactors are the products of self-hydroxylation of tyrosines (e.g., in the copper amine oxidases (*18*)) or tryptophans (e.g., in methylamine dehydrogenase (*19*)) within the protein through metal-assisted catalysis. The F208Y Dopa formation reaction may in some respects serve as a model for the formation of such cofactors.

Methane monooxygenase catalyzes the first and rate-limiting step of carbon fixation in obligate methanotrophic bacteria by converting methane to methanol (*6*). The soluble MMO is comprised of three different protein components, a reductase, a coupling protein, and a hydroxylase (MMOH). The hydroxylase is an $\alpha_2\beta_2\gamma_2$ protein, with molecular weight around 245 kDa. Each α-subunit houses a catalytic diiron center which is the site of methane oxidation. The MMOs can oxidize a broad range of hydrocarbons in addition to methane. The oxygen atom inserted into the substrate in this hydroxylase reaction is from dioxygen.

The pathways for oxygen activation are probably very similar in MMO and RNR R2. The MMO diiron site can form a relatively stable Fe(IV)−Fe(IV) intermediate (*6*), which is the species carrying out the two-electron oxidization of the substrate, and in the R2 system an Fe(III)−Fe(IV) species has been suggested to be the active agent, although in this case the reaction is the one-electron oxidation of Tyr122 (*20*). The crystal structures of the hydroxylase of MMO (MMOH) (*5*, *21*, *22*) show that the coordination of the diiron core is very similar to the R2 protein, despite the lack of any other significant sequence homology. Thus, the different reactivities of these related diiron centers are due to subtle differences in the structural environment of their respective diiron centers.

We have determined the structure of the mutant Y122F/E238A R2 protein soaked with iron, which reveals hydroxylation of the neighboring residue Phe208, in a reaction related to the Dopa formation observed in R2 F208Y and to the MMO hydroxylation. To investigate the flexibility of residue 208 in protein R2 and the possible positions at which the hydroxylating oxo−hydroxo−water groups may be bound at the diiron site in both mutants E238A/Y122F and F208Y, we have also determined the structure of mutant F208Y in its diferrous and apo forms.

EXPERIMENTAL PROCEDURES

Construction and Overexpression of Y122F/E238A and F208Y. Plasmid pMK5/E238A, coding for the mutant protein Y122F/E238A, was constructed by subcloning a 1.0 kb *Bam*HI/Asp718 fragment of pTB2/E238A into the large fragment of plasmid pMK5 cut by the same enzymes (*23*). The sequence of the construct was confirmed by dideoxynucleotide chain termination sequencing across the mutations. Expression and purification of the mutant protein from *E. coli* MC1009 transformed with pMK5/E238A and pGP1-2 followed a procedure described before (*23*). The protein was obtained in the iron-free form.

The mutant F208Y was grown and overexpressed in *E. coli* MC1009 cells containing the plasmids pTB2/F208Y and pGP1-2 (*17*). The cells were grown in iron-depleted medium containing 45.4 mM phosphate buffer, pH 7.3, 7.57 μM $(NH_4)_2SO_4$, 0.4% glucose, 610 μM L-leucine, 406 μM $MgSO_4$, 50 μM EDTA, 5 mM $CaCl_2$, 0.6 μM $ZnCl_2$, 60 mM $CuSO_4$, 0.6 μM $MnCl_2$, 0.75 μM $CoCl_2$, 5.9 μM thiamine dichloride, 50 μg/mL carbenicillin, and 50 μg/mL kanamycin. To remove iron ions, the phosphate buffer and the ammonium sulfate, glucose, and leucine solutions were filtered through a chelating Bio-Rex ion-exchange membrane (Bio-Rad) prior to media preparation. All glassware was washed with 0.1 M sulfuric acid to remove trace amounts of iron. The cells were grown in this medium at a temperature of 30 °C to an optical density of $A_{600nm} = 1.1$. At this OD, expression of the *nrdB* gene was induced by increasing the temperature to 42 °C. After 2.5 h and at $A_{600nm} = 1.4$, the cells were harvested. Since Fe^{3+} does not enter the diiron site, it was no longer necessary to keep solutions iron free after disintegration of the cells. The protein was obtained at more than 90% purity, as described previously (*17*), and contained approximately 0.2−0.3 equiv of Fe per R2 dimer, compared to 2.7−2.8 for iron-containing protein. A further purification step on a MonoQ column immediately prior to crystallization greatly improved the quality of the crystals.

Crystal Soaking and Data Collection. Both mutants were crystallized as described previously (*24*) and the crystals belonged to spacegroup $P2_12_12_1$.

A crystal of apo Y122F/E238A, of dimensions 1.1 × 0.3 × 0.3 mm, was soaked in 1 mL of mother liquor containing 50 mM $FeCl_2$ for 2 h in a 24-well Falcon tissue culture plate sealed with a glass cover slip. A large amount of precipitate formed during the soaking step, presumably iron oxide. The crystal was removed and soaked for less than 1 min in the mother liquor containing additional 20% glycerol, but lacking $FeCl_2$, prior to flash-freezing in a stream of liquid nitrogen at −170 °C. Diffraction data were collected at station 7.2 of the Daresbury Synchrotron Radiation Source (Daresbury Laboratory, Warrington, U.K.), on a MarResearch image plate, used for all data described here. The crystal diffracted to beyond 1.7 Å, but time restrictions limited data collection to around 2.1 Å.

Data for apo F208Y were collected at station X31 of the EMBL outstation at DESY in Hamburg. These crystals diffracted to 2.0 Å. Data were collected to a resolution of 2.1 Å. For iron-containing F208Y, apo F208Y crystals were soaked in 50 mM $FeCl_2$ in Ar-bubbled mother liquor for 3 h before data collection. The crystals were soaked in the $FeCl_2$ solution in a Petri dish. No effort was made to keep the solutions under nonoxidizing conditions during the soak. The X-ray source used was a Siemens rotating anode device.

All data were integrated using the program Denzo and scaled using Scalepack (*25*). Intensities were converted to amplitudes and placed on an absolute scale using the method of French and Wilson (*26*). The Wilson *B* factor (*27*) for all three data sets was around 25 Å^2. A summary of data quality is presented in Table 1.

Model Building and Refinement. The structure of diferrous R2 at 100 K, including solvent molecules (*15*), was used as a starting model for refinement of mutant Y122F/E238A, using the program TNT (*28*, *29*). No restraints on metal−metal or ligand−metal distances were applied during refinement, except that close contact distances between iron and ligand O and N atoms were defined at 1.2 Å, a value significantly less than any actual refined distance. The initial

Table 1: Data Collection Statistics for F208Y and Y122F/E238A[a]

	iron-soaked F208Y	apo F208Y	iron-soaked Y122F/E238A
wavelength (Å)	1.5418	1.07	1.488
cell parameters *a*,*b*,*c* (Å)	73.8, 83.9, 113.5	73.8, 84.2, 114.0	74.1, 83.8, 114.0
resolution range (Å)	20−2.32	20−2.11	27−2.05
completeness (%)	86.5	92.0	98.3
multiplicity of observation	2.1	2.4	3.7
mean $I/\sigma(I)$	10.2	12.0	16.4
R_{merge} (%)	6.8	6.8	8.1

[a] $R_{merge} = \sum_{hkl}\sum_i||F_{o,i}| - \langle|F_o|\rangle|/\sum_{hkl}/\sum_i|F_{o,i}|$, where $|F_{o,i}|$ are the *i* individual observations of each reflection *hkl*, and $<|F_o|>$ is the value after weighted averaging.

R factor was 30.3%, with $R_{free} = 31.8\%$ (*30*) in the range 25−2.8 Å. R_{free} was calculated on 4% of the data (1761 reflections). The resolution limit was increased stepwise to a final value of 2.05 Å. Occupancies for atoms beyond C_β in the side chain of residue Glu238 were set to zero in the initial stages, and no residual density appeared in $2|F_o| - |F_c|$ or $|F_o| - |F_c|$ maps. Model rebuilding, including placement of new water molecules, was carried out using QUANTA (Molecular Simulations Inc.). Maps were calculated using TNT and programs from the CCP4 (*31*) and BIOMOL (Protein Crystallography Group, University of Groningen, The Netherlands) suites. Water molecules with *B* factors exceeding 70 Å^2 were removed, and new water molecules were added at peaks higher than 4σ in difference maps, in several cycles.

Mercury atoms are essential for crystallization of R2 but are occupied to a varying extent in different structures. Almost all of the 12 Cys residues in R2 bind Hg atoms, mostly with low occupancy (*32*). Many have alternate conformations binding two low occupancy Hg atoms. A rough occupancy was decided based on the basis of the height of the peak in a difference map (lying within 2.5 Å of the cysteine Sγ atom), which was altered interactively to give a *B* factor similar to the surrounding protein residues. At some stages, the occupancies of the 15 Hg atoms were refined automatically, while their *B* factors were held constant.

After 62 cycles of TNT refinement, the *R* factor was 21.0% between 25 and 2.5 Å, with $R_{free} = 28.2\%$. All four iron sites were clearly fully occupied. Clear peaks appeared in $|F_o| - |F_c|$ maps at both centers for a bridging monatomic ligand and for a terminal ligand on Fe1 of subunit A (at 8.1σ, 7.6σ, and 4.4σ, respectively). Both were modeled as oxygen atoms and refined with *B* factors around 18 Å^2. Since the crystallization medium contains 0.2 M NaCl, we tried to determine whether the bridging ligand might be a chloride. With Cl^- at both centers, the *B* factors (with occupancy 1.0) or occupancies (with $B = 18$ Å^2) were refined. In the former case the *B* factor rose to 57 Å^2, and in the latter, the occupancy dropped to 0.55 after six further cycles. We are thus confident that the atoms in question are indeed oxygen.

After 103 cycles, R_{model} was 19.4% and R_{free} was 26.9%. The $2|F_o| - |F_c|$ density for residue Phe208 showed bulges in the plane of the aromatic ring suggesting hydroxylation at the C_ϵ position, with a peak at 5.0σ in the corresponding difference map. The distance from the peak center to C_ϵ was consistent with a covalent C−O bond. The residue was refined as ϵ-hydroxy phenylalanine with appropriate changes to the TNT geometry file based on the parameters of Engh and Huber (*33*). An ideal C_ϵ−O bond length of 1.368 Å was used, and the C_ζ−C_ϵ−O and C_δ−C_ϵ−O bond angles were set to 120.2°.

Table 2: Refinement Statistics for the F208Y and Y122F/E238A Models[a]

	iron-soaked F208Y	apo F208Y	iron-soaked Y122F/E238A
resolution range (Å)	13−2.3	13−2.1	15−2.05
no. of reflections	28007/2108	42171/2073	43712/1761
R_{model} (%)	21.6	19.6	19.2
R_{free} (%)	30.9	27.0	26.7
no. of atoms			
total	5877	5873	5941
protein	5594	5594	5575
solvent	264	264	346
Fe	4	0	4
Hg	15	15	16
rms deviations from ideal geometry			
bonds (Å)	0.014	0.015	0.013
angles (deg)	2.2	2.4	2.0
torsion angles (deg)	18.1	16.8	16.8
Ramachandran plot (%)			
core	93.6	92.2	93.1
allowed	6.2	7.6	6.7
generous	0.2	0.2	0.2
mean *B* factors (Å^2)			
main-chain	32.7	29.3	27.8
side-chain	40.5	37.7	36.0
solvent	48.2	40.3	41.8

[a] The geometry library used was that of Engh and Huber (*33*). The second number in the reflection column refers to the number used for R_{free} calculations. $R_{model} = \sum_{hkl}||F_o|_{hkl} - |F_c|_{hkl}|/\sum_{hkl}|F_o|_{hkl}$, where $|F_o|_{hkl}$ is the observed structure factor for reflection *hkl* and $|F_c|_{hkl}$ is the structure factor calculated from the current model. The definitions of core, generous, and allowed areas of the Ramachandran plot are by Morris et al. (*51*).

The hydroxyl oxygen of (ϵ-OH)Phe208 refines with normal *B* factors when given an occupancy of 1.0, which is not due to *B* factor restraints used in refinement since, if Phe122 is refined as Tyr, the hydroxyl oxygen develops high *B* factors despite the same restraints. This suggests that hydroxylation of the Phe208 residues of the subunits A in the crystal is close to complete.

Both variants of F208Y were refined using the same starting model and an essentially identical protocol to that described for Y122F/E238A. Final statistics for all models are presented in Table 2.

Reactivation of Y122F/E238A in Solution. Mutant apo Y122F/E238A or apo E238A in MES buffer (pH 6.8) were reconstituted with 4 mol of ferrous ammonium sulfate per mol of R2 and, where appropriate, 16 mol of ascorbate per mol of R2. These reactivations were also carried out in the presence of 1 M formate or 1 M acetate. Spectra were recorded on a Perkin-Elmer Lambda-2 scanning spectrophotometer, and the absorbance of the apo protein, recorded immediately before reconstitution, was subtracted.

RESULTS

Structure of the Y122F/E238A Mutant. The overall structure of Y122F/E238A is very similar to other forms of R2, and the rms deviation in C_α atoms between Y122F/E238A and wild-type R2 is 0.32 Å. However, the structure

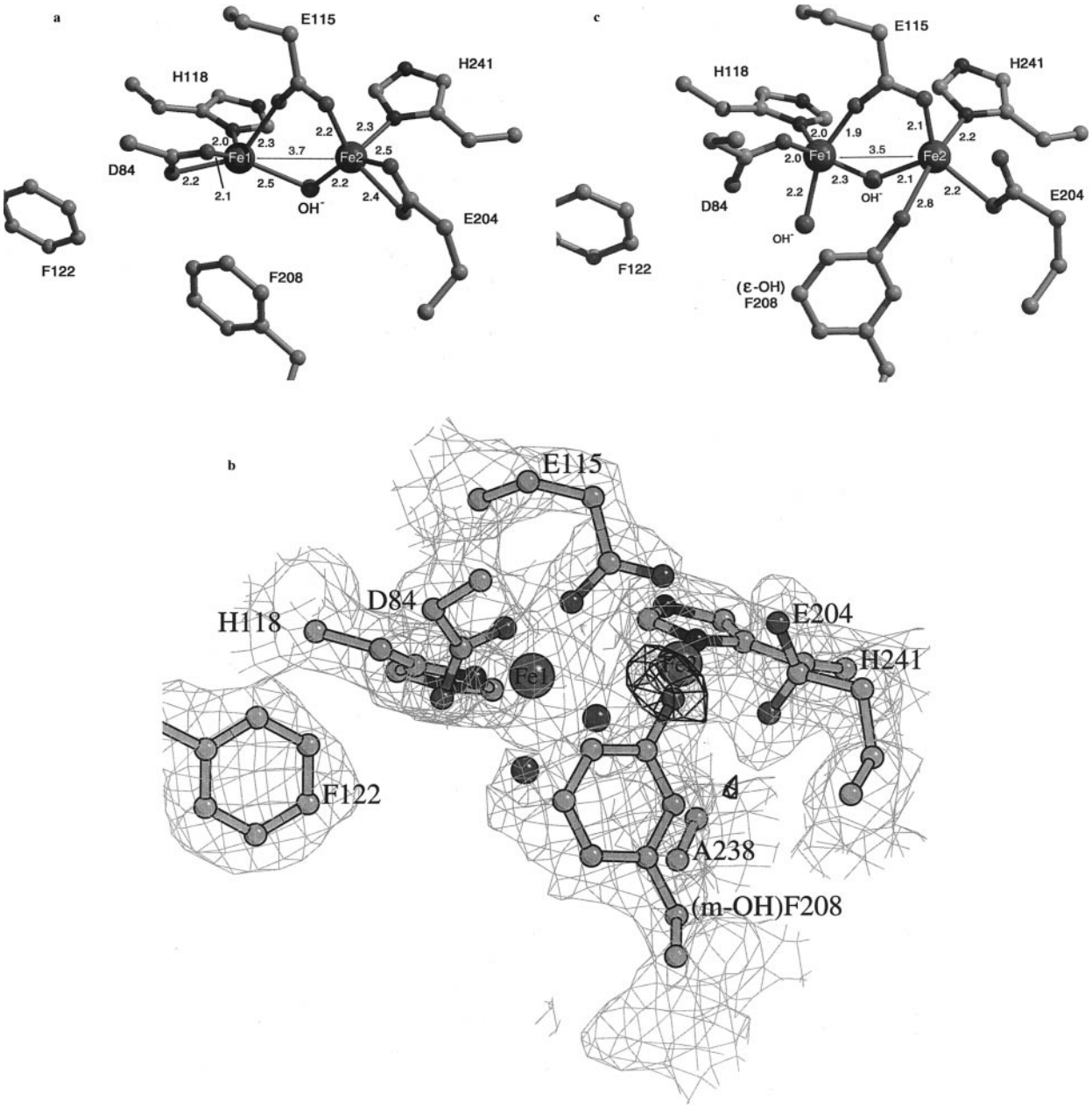

FIGURE 1: (a) Iron coordination in subunit B of R2 mutant Y122F/E283A. The iron−iron and iron−ligand distances are given in Ångströms. The iron ions are displayed as CPK spheres, and the other atoms are in ball-and-stick representation. (b) Electron density, with final atomic model superimposed, for the diiron center in subunit A of Y122F/E238A, using phases derived from the final model, but with certain atoms omitted from the phasing. A $2|F_o| - |F_c|$ map is shown in thin gray lines, contoured at 0.9σ; all displayed atoms are absent from the phasing model. An $|F_o| - |F_c|$ map is shown in thicker black lines, contoured at 3.5σ. In this case only the extra oxygen atom on the ϵ-hydroxylated Phe208 has been omitted. Both maps are contoured to cover all the displayed atoms. (c) Iron coordination in subunit A of Y122F/E238A. The color scheme is the same as for Figure 1a. The nomenclatures m-OH and ϵ-OH are equivalent.

of the diiron sites is different from that seen in any other R2 form, and the structure in the two crystallographically independent subunits is significantly different. This reactive asymmetry has also been seen in the chemical reduction of a mutant R2 (*15*) and in the reconstitution of apo R2 with cobalt (Nordlund, unpublished results). This is most likely due to differences in accessibility to low molecular weight compounds because of crystal packing effects on subunit B (*32*).

Structure of the Diiron Site in Subunit B. The coordination of the diiron site in subunit B is shown in Figure 1a. Both iron ions are pentacoordinate, bound to one terminal bidentate carboxylate and one terminal histidine each and bridged by one carboxylate and one low molecular weight ligand. The latter is, to judge by its distances to the iron atoms, either a μ-hydroxo or a μ-water bridge but not a μ-oxo bridge. Assuming that the net charge of this site is zero, which has been the case for all other R2 sites for which structures have been determined (*15*, *17*, *34*−*37*), the most plausible redox state is a hydroxo-bridged diiron site with the two iron ions in the ferrous form. This is also consistent with the Fe−Fe distance of 3.7 Å. We have also considered the possibility that the bridging low M_r species is a chloride anion, since NaCl is present at a concentration of 0.2 M in the crystallization solution. However, refinement of the structure with a chloride ion in this position gave high *B* factors. Although this could also be explained by low occupancy, this would be reflected in a mixed population of iron sites with different

oxidation states, and the well-defined electron density is not consistent with such a mixture.

Most features of the second coordination sphere of the iron ions found in the wild-type protein are present in diferrous Y122F/E238A. Two water molecules present in the diferric protein on the side of Glu204 distal from the iron center are not present in diferrous wild-type R2, where the iron−iron distance has expanded from 3.3 to 3.9 Å (*15*). They are also absent here. Phe208, the residue in the hydrophobic pocket located closest to the diiron site, has appeared to be relatively flexible in different structures of R2, having comparatively high *B* factors for a buried residue and correspondingly poorly defined electron density. However, in diferrous Y122F/E238A, the density for Phe208 is clear, and the side chain refines to a position similar to that in diferrous wild-type R2. The closest distance between the iron ions and Phe208 is between C_ϵ and Fe2 (3.8 Å). The closest approach to Fe1 is 5.1 Å.

Structure of the ϵ-Hydroxyphenylalanine Coordinated Diiron Site in Subunit A. To our surprise, Phe208 in subunit A has clearly been hydroxylated at the meta, or ϵ-, ring position (Figure 1b,c). The inserted oxygen atom coordinates Fe2 at a rather long distance of 2.8 Å and is therefore almost certainly protonated. The iron-coordinating histidine and carboxylate side chains have conformations largely similar to those seen in the diferrous B site, but the terminal carboxylate ligands Asp84 and Glu204 are now monodentate. The site has one additional low M_r ligand coordinated to Fe1 which is not present in subunit B (Figure 1b,c), making both iron ions also pentacoordinate in this site. The iron−iron distance is 3.5 Å, and the lengths of the Fe-bridging moiety bonds are 2.1 and 2.3 Å.

Spectroscopic studies of iron reconstituted Y122F/E238A in solution revealed a broad, weak absorption band in the range 450−550 nm, which became slightly more pronounced with maxima at 475 and 515 nm if excess ascorbate was present in the reconstitution mixture (Figure 2a). Likewise, reconstitution of the single mutant E238A in the presence of ascorbate revealed a weak absorption band at 515 nm (cf. Figure 2b) (*23*) and in the presence of both ascorbate and acetate or formate a weak, rather narrow band at 475 nm (Figure 2b). In wild-type R2, excess ascorbate has been shown not to affect the radical generation but to keep the iron in the ferrous form. For comparison, inclusion of chloride ions has no effect on the reactivation reaction (data not shown). In the case of reconstitution of Y122F/E238A in the crystal form, it now appears that excess iron may influence the oxygen activation reaction in a similar and perhaps more efficient manner since the crystals have a near-stoichiometric yield of (ϵ-OH)F208.

The spectra in Figure 2a,b have the general features of spectra from purple acid phosphatases (PAPs) (*38*) and of phenol bound to the diiron site of MMO (*39*), although the intensity of the absorption bands is lower. In the latter system, a broad absorption centered at 500 nm could be attributed to a phenolate to Fe(III) ligand−metal charge transfer (LMCT). A stronger tyrosinate to Fe(III) LMCT absorption is observed in PAPs. In osteoclast PAP, the broad absorption is centered at 544 or 515 nm, depending on whether the iron center is in the oxidized (Fe(III)−Fe(III)) or reduced, active (Fe(II)−Fe(III)) state, respectively (*40*). The crystal structure of a red kidney bean PAP showed a

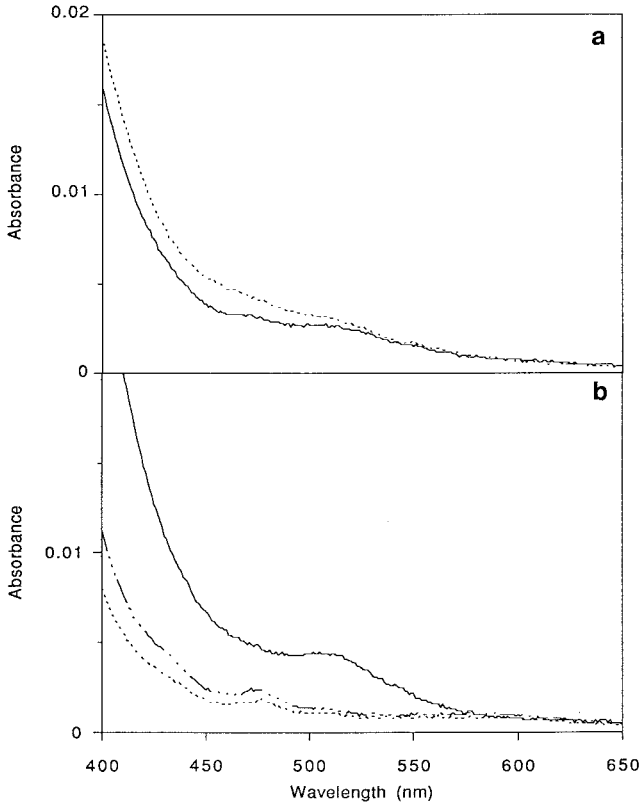

FIGURE 2: Visible absorption spectrum of reactivated Y122F/E238A and E238A mutant proteins after reconstitution in solution at pH 6.8. (a) Y122F/E238A (10 μM) reconstituted in MES buffer for 90 min (solid line) and with ascorbate for 60 min (dotted line). (b) E238A (10 μM) reconstituted in MES buffer with ascorbate (solid line); with addition of 1 M acetate (dash−dotted line); and with addition of 1 M formate (dotted line). These spectra were recorded after 10 min of reconstitution.

Tyr residue coordinating an Fe(III) atom at a distance of 2.1 Å (*11*). The relative weakness of the absorption seen in Y122F/E238A is in apparent contradiction with the fact that the crystal structure suggests hydroxylation of the majority of the Phe208 residues of subunit A in the crystal. However, the absorption may be weak due to the relatively long coordination distance (2.8 Å) compared to that in PAP. It may also be that movement of Phe208 is slightly more restricted in the crystal than in solution, which permits a higher degree of hydroxylation. Nevertheless the visible absorption spectrum clearly confirms hydroxylation of Phe208.

The slightly shorter iron−iron and iron-bridging moiety bond lengths in subunit A suggest that the oxidation number of the iron center is at least one unit higher than in subunit B. According to the zero net charge preference of R2 metal clusters (*36*), this would suggest that the center is (a) Fe(II)·Fe(III)·$2OH^-$, (b) Fe(III)·Fe(III)·O^{2-}·OH^-, or (c) Fe(II)·Fe(II)·OH^-·H_2O. The Fe-bridging moiety distances are too long for an oxo bridge, which makes b unlikely. Electron paramagnetic resonance studies of the single mutant E238A in solution support the stability of a mixed-valent state over a period of up to 2 h (R. Davydov, B. O. Persson, et al., unpublished). In PAPs, the LMCT-derived absorption, similar to that seen here, has been shown to derive from Tyr coordination to the nonredox active Fe, which remains in the Fe(III) state in both reduced and oxidized mammalian PAP. In addition, spectroscopic results suggest the presence

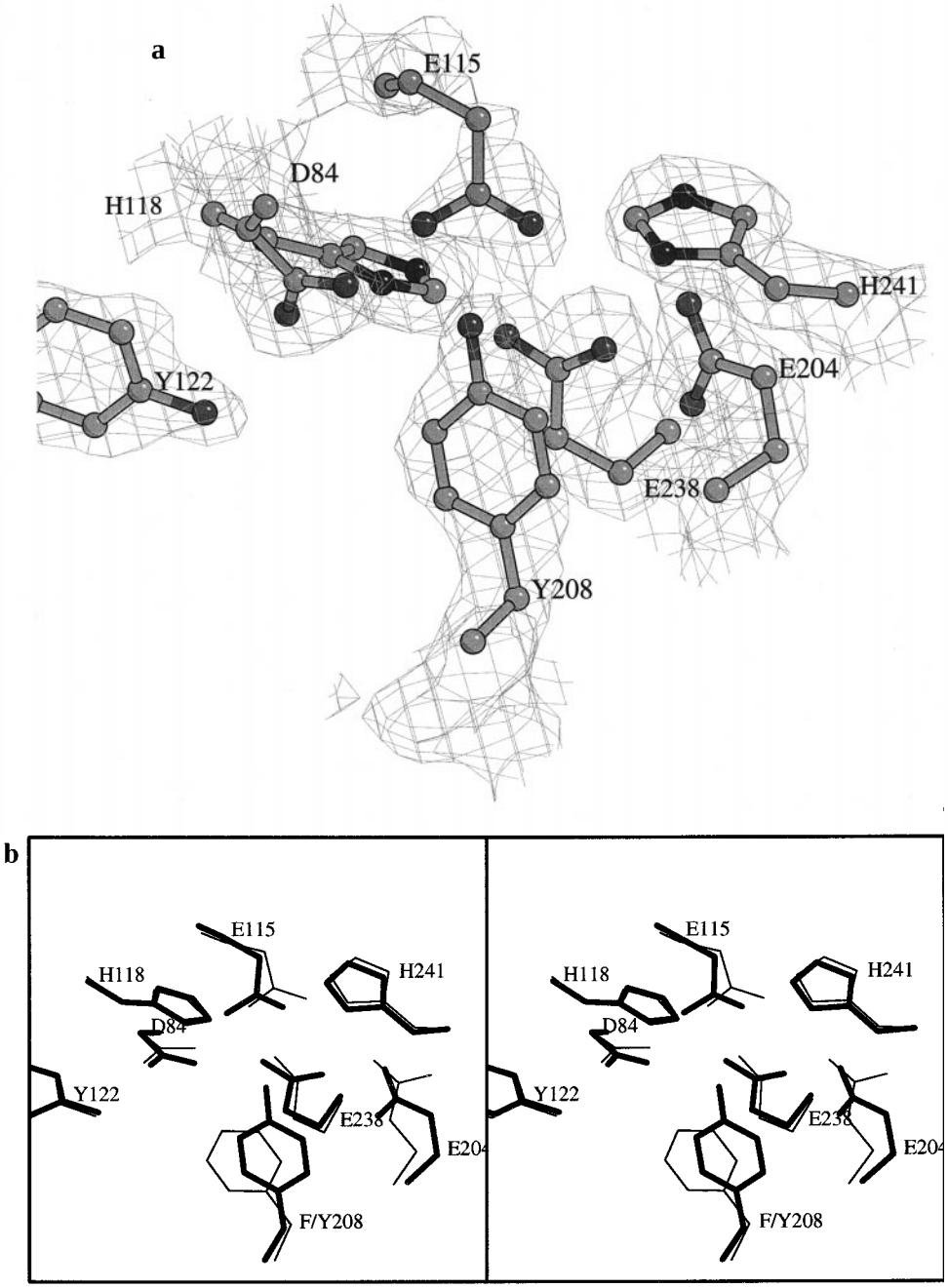

FIGURE 3: (a) $2|F_o| - |F_c|$ electron density for the future diiron site of apo F208Y, with the final atomic model superimposed. All displayed atoms are omitted from the phasing. The map is contoured at 1.0σ. (b) Divergent stereoview of the empty "iron site" structure of apo F208Y (thick lines) superimposed on that of wild-type apoR2 (thin lines).

of a terminal hydroxo ligand in PAPs (*41*, *42*). Taken together, this evidence favors the Fe(II)−Fe(III) state for subunit A of Y122F/E238A, and we have depicted it as such in Figure 1c, although the Fe(II)−Fe(II) state cannot be totally excluded.

Structures of Apo and Diferrous F208Y. The structures of the apo and diferrous forms of the mutant F208Y are both very similar to the corresponding wild-type R2 structures, with rms deviations in C_α positions between apo wild-type (*36*) and apo F208Y of 0.37 Å and between diferrous wild-type (*15*) and iron-soaked F208Y of 0.42 Å. The main differences are restricted to the immediate surroundings of the diiron site. Despite a trace of iron at the Fe2 position (less than 20%), the geometry of the future iron ligands is well defined by the electron density in the nascent iron site of apo F208Y and is very similar to that of apo wild-type R2 (Figure 3a,b). The carboxylate residues are clustered together, and two of them are presumably protonated which, together with the double protonation of the future histidine ligands, gives a neutral diiron site. Tyr208 makes similar interactions to those made by F208 in wild-type apo R2, but in addition, the OH group makes a hydrogen bond to Asp84.

Iron-containing F208Y was generated semiaerobically with a large excess of ferrous iron. In subunit B, the occupancy of one of the iron ions (Fe1) is only 50%, making the detailed structure of this site hard to elucidate. These results suggest that iron diffusion into subunit B in the crystalline phase is rather slow. The iron coordination in subunit A is similar to that seen in wild-type diferrous protein (Figure 4a,b), with Glu115 and Glu238 as the sole bridging ligands and an iron−

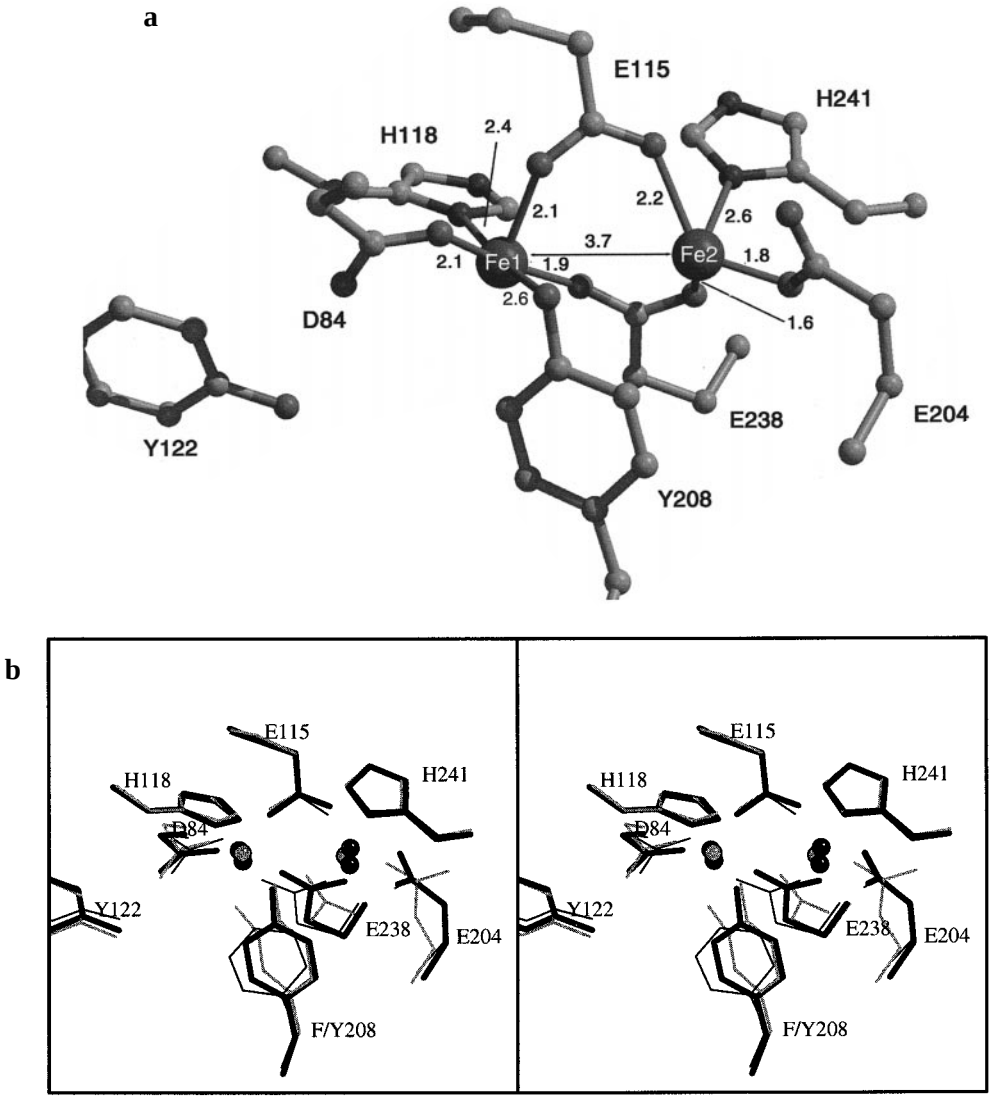

FIGURE 4: (a) Schematic structure of diferrous F208Y. Coordination distances are shown in angstroms. (b) Stereoview of the diiron center of diferrous F208Y (thick black lines) superimposed on that of wild-type diferrous R2 (thin black lines) and that of diferric Dopa208 (medium gray lines).

iron distance of 3.7 Å. Tyr208 now coordinates Fe1 at a distance of 2.6 Å. It is clear from the electron density maps that the tyrosine is not further hydroxylated to Dopa. The oxygen of the Tyr208 side chain is in a similar position to O4 in Dopa208 R2, although the rings have slightly different orientations (Figure 4b). In Dopa208 R2, Glu238 is a bidentate ligand to Fe2 yet is in a similar position to diferrous F208Y, where it is a fully bridging ligand. The conformations of Glu238 in the reduced and oxidized F208Y mutants are very different from those in the wild-type structures, and it appears that coordination of Tyr208 or Dopa208 to the iron site generates steric hindrance for Glu238, preventing it from going through its regular carboxylate shift upon oxidation (*15*).

DISCUSSION

Structural studies of different forms of the R2 diiron site have revealed that Fe1 is relatively fixed in relation to the rest of the protein, while Fe2 moves more easily, e.g., upon reduction. This is because Fe1 is coordinated to the terminal Asp84, which has a low flexibility and is in a dense part of the protein matrix, while Fe2 is coordinated to Glu204, which is more flexible and in a less dense environment containing water molecules. In wild-type R2 structures, Glu238 has also been observed to be an unusually flexible metal ligand; the same is true for the corresponding residue in MMO, Glu243. In the diferrous form of reduced R2, Glu238 follows the pseudo 2-fold symmetry of the diiron sites, but in the diferric form of R2 and in all forms of MMO, the symmetry of the site is broken by this particular Glu residue. The reason the symmetry is broken in one particular direction is probably a combination of the availability of space for the side chain of Glu238 to move together with forces from the helix framework that prevent the side chain from reaching a symmetric position in the diferric form of R2, where the Fe atoms are closer together. The asymmetry may be important, as the diiron site should favor oxidation reactions at Fe1, which is in close vicinity to Tyr122. In Y122F/E238A, the absence of the side chain of Glu238 opens space for structural changes at the diiron site which are probably not possible in the wild-type protein. Distortion of the asymmetry, which in wild-type R2 presumably steers the reaction toward oxidation of Tyr122, might lead to the hydroxylation of Phe208 in Y122F/E238A.

The three structures of different forms of the F208Y mutant, namely apo F208Y, diferrous F208Y, and Dopa208, show similar positions for Tyr208, and in the iron containing forms, the phenolic oxygens coordinate the relatively rigid Fe1. This suggests that Tyr208 will be locked onto Fe1 in this way all through the reaction cycle, which will leave only one-dimensional freedom for Tyr208, through the χ_2 dihedral angle. As an effect of the restricted movement of Tyr208, Glu238 cannot accommodate its normal carboxylate shift to full monodentate ligation to Fe2 but will instead be restricted to more hindered coordination modes similar to those observed in diferric and diferrous F208Y (Figure 4a,b). However, this does not prevent formation of some Tyr122$^\bullet$, as has been demonstrated by two groups (*16*, *17*, *43*).

What could be the mechanism leading to hydroxylation of the ϵ-carbon in each of these mutants? Considering the distance from residue Phe208 to the iron atoms in Y122F/E238A and its limited rotational freedom, a direct carbon−iron bond as an intermediate, as proposed for methane hydroxylation by MMO (*44*), is unlikely in this case. However, the oxo−hydroxyl−water groups (OHW) coordinated to the iron site in the high valent forms will be important players in the hydroxylation reaction. They could be seen as having two types of potential function, first as activators of the substrate through electron, proton, or hydrogen abstraction and second as possible nucleophiles, to be inserted into the substrate. Nevertheless, in the case of F208Y, where Tyr208 is coordinated to the diiron site, a direct electron transfer generating a tyrosyl radical is also a possible mechanism for substrate activation. In any case, the oxygen species inserted into the tyrosine ring will most probably be coordinated to the iron center, since the reaction appears to be highly specific.

The hydroxylation reaction in Y122F/E238A most likely utilizes a mechanism involving hydrogen abstraction. The hydroxylation of Phe208 is presumably much harder to achieve than that of Tyr208 in F208Y. For example, in CH_3CN, the oxidation potential of Phe is more than +1.8 V as opposed to +1.3 V for Tyr (*45*). The hydroxylation observed in Y122F/E238A possibly represents an uncoupling which allows a hydroxo or oxo species not present in the wild-type protein to be exposed in the mutant diiron site. This species could mediate the hydrogen abstraction and, in a subsequent step, the hydroxylation of Phe208, possibly through a rebound mechanism as suggested for MMO (*6*). The hydroxylation of Phe208 in Y122F/E238A further underlines the relatedness of the dioxygen activation reactions in MMO and RNR R2 and the importance of specifically directing the oxidative power of the cluster toward oxidation of Tyr122 in R2 rather than harmful oxidation of other neighboring residues.

On the basis of structural studies of diiron proteins, several different possible OHW binding sites can be predicted for the diiron sites of E238A/Y122F and F208Y (Figure 5). They can be roughly divided into the locations of (A) the oxo bridge in metR2, facing away from the hydrophobic pocket (this site is equivalent to one of the hydroxo bridges in MMO), (B) the second hydroxo bridge in MMO, (C) the water ligand on Fe1 in metR2, and (D) the water ligand on Fe2 in metR2. Positions B−D are exposed in the hydrophobic pocket. Which of these are involved in activating the substrate and are the source of the oxygen inserted into

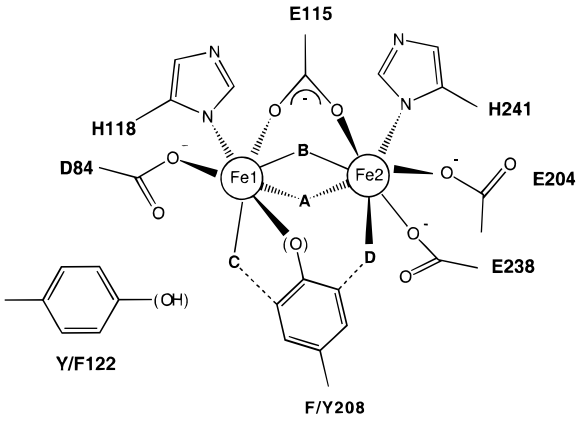

FIGURE 5: A schematic diagram illustrating a set of possible oxo−hydroxo−water (OHW) positions (bold letters A−D) on the R2 diiron site which might be involved in hydrocarbon activation and/or oxidative insertion into the Tyr or Phe208 ring. The dotted lines indicate the most likely sites for oxygen insertion.

the ring in the two mutants? Considering our structures, position A is not likely to be involved since it is not exposed to the hydrophobic pocket. Position B is also unlikely to be the source since, in F208Y, it appears to be sterically hindered by the oxygen of Tyr208 and, in Y122F/E238A, it is remote from the final site of hydroxylation. As judged from the present structures, position C is the most likely for F208Y, and position D is the most likely for Y122F/E238A. In fact, comparison with the coordinating water positions in metR2 shows that the inserted oxygens of Dopa208 and (ϵ-OH)Phe208 lie very close to positions C and D in the respective mutants. These positions are also the most accessible to penetrating solvent molecules in R2 (*2*, *15*) which could explain why the inserted oxygen in F208Y is not derived from dioxygen. The accumulation of reactive intermediates in F208Y is much slower than in wild-type R2 (*17*), which allows terminal Fe ligands derived from O_2 to exchange with solvent (*46*). However, the possibility of hydroxylation by an OHW species derived from molecular oxygen has not been excluded for Y122F/E238A.

What can be the relationship between the proposed OHW species in the reactions catalyzed by these mutant proteins and the intermediate **X** observed for wild-type and some mutant R2s? **X** is the species catalytically competent to oxidize Tyr122 (*47*) and is best formally described as an Fe(III)−Fe(IV) center with substantial delocalization of the spin onto the oxygen ligands (*20*). The two-electron oxidations of Y208 and F208 in the respective mutants resemble strongly the reaction carried out by MMOH and are most likely to be caused by an asymmetrical Fe(IV)−Fe(IV) center, presumably an as yet unobserved precursor of **X**. It was recently shown that γ-irradiation of the Fe(IV)−Fe(IV) intermediate Q in MMOH at 77K could produce a species with Mössbauer properties very similar to those of **X** (48). This further underlines the extreme similarity between the MMOH and R2 diiron centers and the necessity for specific direction of the oxidative power in R2.

Our structural data suggest that the OHW species hydroxylating Tyr208 in mutant F208Y is closer to the "normal" situation in wild-type R2 where a reactive high-valent species is exposed on Fe1 near Tyr122 and, conversely, that E238A/Y122F resembles a "defective" activation where it is allowed to be exposed on the wrong Fe atom,

namely Fe2, due to its less saturated coordination caused by the absence of Glu238. This implies an important role for Glu238 in directing the oxidative chemistry and protecting R2 from damaging autoxidation.

Bollinger et al. have exploited the observation that Fe^{2+} binds preferentially to the Fe2 position at low Fe/R2 ratios and ^{57}Fe Mössbauer experiments to demonstrate that, in contrast to what might be expected, the high-valent species of **X** is most likely located on Fe2 rather than on Fe1 (*49*). Our results on F208Y confirm preferential Fe(II) binding: in the apo form we see 20% Fe at Fe2 and none at Fe1; in the diferrous form there is only 50% Fe at Fe1 in one of the subunits, while both Fe2 sites have full occupancy. The same workers have shown that the equilibrium between Tyr122 radical (one-electron oxidation) and Dopa208 (two-electron oxidation) in F208Y can be affected by the concentration of ascorbate (a one-electron donor) or by mutation of the surface residue Trp48 to Phe. The W48F mutation breaks an electron transfer pathway from the exterior of R2, where an electron, e.g., from ascorbate, would enter, which is also consistent with a mechanism in which an initial Fe(IV)−Fe(IV) center is rapidly reduced to Fe(III)−Fe(IV) by injection of an external electron (*43*). Since this pathway includes Fe1, it would be a likely candidate for the Fe(III) species. However, for a hydroxylation event to take place on Fe1, we consider that this intermediate [i.e., Fe1(III)−Fe2(IV)] should be in very close equilibrium with a high-valent species on the same atom, as suggested by our results. Recent rapid freeze−quench (RFQ) EXAFS data demonstrate that the Fe−Fe distance in **X** is as low as 2.5 Å, which suggests one or more bridging monodentate carboxylate ligands in addition to the oxo bridge (*50*). Due to the compact nature of the intermediate, we could thus consider the oxidation states of this iron center to be more fluid than a clear Fe1(III)−Fe2(IV) partition.

In any case, it is clear that these R2 mutants need further studies in order to determine their exact reaction mechanisms as well as the relationship of the above mechanisms to those of the MMO related systems. In particular, the molecular origin of the inserted oxygen atom in E238A should be established. However, we feel that the engineered R2 hydroxylases, due to their conformationally restricted substrates, are potentially a very important system for revealing structural details of the geometry of diiron-catalyzed hydroxylation reactions, information that might be hard to obtain from the true diiron hydroxylases.

ACKNOWLEDGMENT

We thank staff at the Daresbury SRS and at the Hamburg outstation of the EMBL at DESY for technical assistance and Dr. Marjolein Thunnissen for practical help with data collection. We thank Prof. Astrid Gräslund and her group for stimulating discussion regarding the manuscript.

NOTE ADDED IN PROOF

Liu et al. (*56*) have very recently described a new paramagnetic EPR species in mutant F208Y, termed Z. They postulate that this arises from an Fe1(IV)−Fe(III)-like intermediate in which the high-valent Fe1 is stabilized by interaction with Y208.

REFERENCES

1. Nordlund, P., and Eklund, H. (1996) *Curr. Opin. Struct. Biol. 5*, 758−766.
2. Nordlund, P., Sjöberg, B.-M., and Eklund, H. (1990) *Nature 345*, 593−598.
3. Fontecave, M., Nordlund, P., Eklund, H., and Reichard, P. (1992) *Adv. Enzymol. Relat. Areas Mol. Biol. 65*, 147−183.
4. Sjöberg, B. M. (1997) *Struct. and Bonding* 88, 139−173.
5. Rosenzweig, A. C., Frederick, C. A., Lippard, S. J., and Nordlund, P. (1993) *Nature 366*, 537−543.
6. Lipscomb, J. D. (1994) *Annu. Rev. Microbiol. 48*, 371−399.
7. Lindqvist, Y., Huang, W., Schneider, G., and Shanklin, J. (1996) *EMBO J. 15*, 4081−4092.
8. Frolow, F., Kalb(Gilboa), J., and Yariv, J. (1994) *Nat. Struct. Biol. 1*, 453−460.
9. deMaré, F., Kurtz, D. M. J., and Nordlund, P. (1996) *Nat. Struct. Biol. 3*, 539−546.
10. Stenkamp, R. E. (1994) *Chem. Rev. 94*, 715−726.
11. Sträter, N., Klabunde, T., Tucker, P., Witzel, H., and Krebs, B. (1995) *Science 268*, 1489−1492.
12. Ling, J. S., Sahlin, M., Sjöberg, B. M., Loehr, T. M., and Sanders-Loehr, J. (1994) *J. Biol. Chem. 269*, 5595−5601.
13. Sahlin, M., Lassmann, G., Pötsch, S., Sjöberg, B. M., and Gräslund, A. (1995) *J. Biol. Chem. 270*, 12361−12372.
14. Katterle, B., Sahlin, M., Schmidt, P. P., Pötsch, S., Logan, D., Gräslund, A., and Sjöberg, B. M. (1997) *J. Biol. Chem. 272*, 10414−10421.
15. Logan, D. T., Su, X.-D., Åberg, A., Regnström, K., Hajdu, J., Eklund, H., and Nordlund, P. (1996) *Structure 4*, 1053−1064.
16. Ormö, M., deMaré, F., Regnström, K., Åberg, A., Sahlin, M., Ling, J., Loehr, T. M., Sanders-Loehr, J., and Sjöberg, B. M. (1992) *J. Biol. Chem. 267*, 8711−8714.
17. Åberg, A., Ormö, M., Nordlund, P., and Sjöberg, B. M. (1993) *Biochemistry 32*, 9845−9850.
18. Klinman, J. P., and Mu, D. (1994) *Annu. Rev. Biochem. 63*, 299−344.
19. Hartmann, C., and McIntire, W. S. (1997) *Methods Enzymol. 280*, 98−150.
20. Sturgeon, B. E., Burdi, D., Chen, S., Huynh, B.-H., Edmondson, D. E., Stubbe, J., and Hoffman B. M. (1997) *J. Am. Chem. Soc. 118*, 7551−7557.
21. Rosenzweig, A. C., Nordlund, P., Takahara, P. M., Frederick, C. A., and Lippard, S. J. (1995) *Chem. Biol. 2*, 409−418.
22. Rosenzweig, A. C., Fredrick, C. A., and Lippard, S. J. (1996) in *Microbial Growth on C1 Compounds: proceedings of the 8th International Symposium on Microbial Growth on C1 Compounds* (Lidstrom, M. E., and Tabita, F. R., Eds.) 141−149, Kluwer, Dordrecht, The Netherlands.
23. Persson, B. O., Karlsson, M., Climent, I., Ling, J. S., Sanders-Loehr, J., Sahlin, M., and Sjöberg, B. M. (1996) *J. Biol. Inorg. Chem. 1*, 247−256.
24. Nordlund, P., Uhlin, U., Westergren, C., Joelsen, T., Sjöberg, B. M., and Eklund, H. (1989) *FEBS Lett. 258*, 251−254.
25. Otwinowski, Z. (1993) in *Data collection and Processing. Proceedings of the CCP4 study weekend.* 56−62, SERC Daresbury Laboratory, Warrington, U.K.
26. French, S., and Wilson, K. S. (1974) *Acta Crystallogr. A34*, 517−523.
27. Wilson, A. J. C. (1949) *Acta Crystallogr. 2*, 318−321.
28. Tronrud, D. E., ten Eyck, L. F., and Matthews, B. W. (1987) *Acta Crystallogr. A43*, 481−501.
29. Tronrud, D. E. (1992) *Acta Crystallogr. A48*, 912−916.
30. Brünger, A. (1992) *Nature 355*, 472−475.
31. Collaborative Computational Project, no. 4 (1994) *Acta Crystallogr. D50*, 760−763.
32. Nordlund, P., and Eklund, H. (1993) *J. Mol. Biol. 232*, 123−164.
33. Engh, R. A., and Huber, R. (1991) *Acta Crystallogr. A47*, 392−400.
34. Åberg, A. (1993) Ph.D. Thesis, Stockholm University.
35. Atta, M., Nordlund, P., Åberg, A., Eklund, H., and Fontecave, M. (1992) *J. Biol. Chem. 267*, 20682−20688.
36. Åberg, A., Nordlund, P., and Eklund, H. (1993) *Nature 361*, 276−278.

37. Su, X.-D. (1994) Ph.D. Thesis, Stockholm University.
38. Andersson, K. K., and Gräslund, A. (1995) *Adv. Inorg. Chem. 43*, 359−408.
39. Andersson, K. K., Elgren, T. E., Que, L. J., and Lipscomb, J. D. (1992) *J. Am. Chem. Soc. 114*, 8711−8713.
40. Ek-Rylander, B., Barkhem, T., Ljusberg, J., Öhman, L., Andersson, K. K., and Andersson, G. (1997) *Biochem. J. 321*, 305−311.
41. Dietrich, M., Münstermann, D., Suerbaum, H., and Witzel, H. (1991) *Eur. J. Biochem. 199*, 105−113.
42. Suerbaum, H., Körner, M., Witzel, H., Althaus, E., Mösel, B. D., and Muller-Warmuth, W. (1993) *Eur. J. Biochem. 214*, 313−321.
43. Parkin, S. E., Chen, S., Ley, B. A., Mangravite, L., Edmondson, D. E., Huynh, B.-H., and Bollinger, J. M., Jr. (1998) *Biochemistry 37*, 1124−1130.
44. Siegbahn, P., and Crabtree, R. H. (1997) *J. Am. Chem. Soc. 119*, 3103−3113.
45. Isied, S. S. (1994) in *Metal ions in biological systems* (Sigel, H., and Sigel, A., Eds.) 1−50, Marcel Dekker, Inc., New York.
46. Nam, W. W., and Valentine, J. S. (1993) *J. Am. Chem. Soc. 115*, 1772−1778.
47. Bollinger, J. M., Jr., Tong, W. H., Ravi, N., Huynh, B. H., Edmondson, D. E., and Stubbe, J. (1994) *J. Am. Chem. Soc. 116*, 8015−8023.
48. Valentine, A. M., Tavares, P., Pereira, A. S., Davydov, R., Krebs, C., Hoffmann, B. M., Edmondson, D. E., Huynh, B.-H., and Lippard, S. J. (1998) *J. Am. Chem. Soc. 120*, 2190−2191.
49. Bollinger, J. M., Jr., Chen, S., Parkin, S. E., Mangravite, L. A., Ley, B. A., Edmondson, D. E., and Huynh, B. H. (1997) *J. Am. Chem. Soc. 119*, 5976−5977.
50. Riggs-Gelasco, P. J., Shu, L., Chen, S., Burdi, D., Huynh, B. H., Que, L., Jr., and Stubbe, J. (1998) *J. Am. Chem. Soc. 120*, 849−860.
51. Morris A. L., MacArthur M. W., Hutchinson E. G., and Thornton J. M. (1992) *Proteins 12*, 345−364.
52. Esnouf, R. M. (1997) *J. Mol. Graphics 15*, 133−138.
53. Kraulis, P. J. (1991) *J. Appl. Crystallogr. 24*, 946−950.
54. Bacon, D. J., and Anderson, W. F. (1988) *J. Mol. Graphics 6*, 219−220.
55. Merritt, E. A., and Murphy, M. E. P. (1994) *Acta Crystallogr. D50*, 869−873.
56. Liu, A., Sahlin, M., Pötsch, S., Sjöberg, B. M., and Gräslund, A. (1998) *Biochem. Biophys. Res. Commun. 246*, 740−745.

BI9806403